Neutron total cross sections at intermediate energies

R. W. Finlay, W. P. Abfalterer, G. Fink, E. Montei, and T. Adami
Department of Physics and Astronomy, Ohio University, Athens, Ohio 45701

P. W. Lisowski, G. L. Morgan, and R. C. Haight
P-Division, Los Alamos National Laboratory, Los Alamos, New Mexico 87545
(Received 30 September 1992)

Pulsed-beam time-of-flight techniques are used in a transmission measurement with a continuous spectrum of neutrons to determine neutron total cross sections with good precision up to 600 MeV. Neutrons are produced by spallation of the 800 MeV proton beam from the Los Alamos Meson Physics Facility accelerator incident on a thick, heavily shielded tungsten target at the Weapons Neutron Research facility at Los Alamos National Laboratory. Transmission measurements were completed for fifteen elements with $9 \leq A \leq 209$ and three isotopically enriched samples of ^{40}Ca, ^{90}Zr, and ^{208}Pb. Principal features of the experiment are the intensity and time structure of the neutron source, tight collimation of the neutron beam line, good geometry, rapid cycling of the samples, stable electronics, and a small, fast neutron detector. Errors due to counting statistics were generally less than 1% for each of several hundred energy bins for each target. The measurements represent steps in the development of a neutron-nucleus optical potential at intermediate energy and important input for the clarification of isovector effects in the nucleon-nucleus interaction. The data also provide insight into the long-standing discussion of mean free paths of the nucleon in the nucleus.

PACS number(s): 24.10.−i, 25.40.−h, 25.40.Ve, 28.20.Gd

I. INTRODUCTION

Although neutron total cross sections have been under investigation for over 50 years, it is remarkable how few data are available in the intermediate-energy region. The 1988 edition of the Brookhaven "Barn Book" [1] summarizes the situation: Schimmerling *et al.* [2] measured $\sigma_T(E)$ at 15 energies between 379 and 1731 MeV for 12 naturally abundant samples ranging from Be to U. More recently, Franz *et al.* [3] measured $\sigma_T(E)$ for Be, C, O, Al, V, Mn, Co, Cu, Ag, Ce, Ta, Pb, Bi, and U at 22 energies between 160 and 575 MeV. Otherwise, no data set contains more than two points for any nucleus with $12 < A < 208$ except for Si, which has been studied in detail. There is a total lack of neutron cross-section data for the separated isotope targets of interest in intermediate-energy nucleus physics (e.g., ^{40,48}Ca, ^{90}Zr, ^{120}Sn, and ^{208}Pb).

Yet this is a potentially interesting region for nuclear physics: The pion production channel opens, and effects of the pion-nucleon (Δ) resonance become important. Above about 200 MeV, an impulse approximation might be expected to give a good description of the data, while at lower energy Pauli blocking and medium effects must be included. Phenomenologically, the imaginary term in the optical potential increases rapidly, while the real term is thought to pass through zero. There is considerable recent interest in the development of reaction theories at intermediate energy, with much progress in "full-folding models" [4,5], relativistic impulse approximations [6], and Dirac phenomenology [7]. All of these areas would be well served by the availability of more detailed, precise neutron measurements in this energy region.

On a more elementary level, the mean free path of a nucleon in the nucleus remains an elusive concept. Schiffer [8] pointed out that the commonly accepted empirical values of the mean free path were about a factor of 2 larger than the predictions of any *a priori* optical model. Much of the discrepancy was explained by Negele and Yazaki [9] and by Fantoni, Friman, and Pandharipande [10] in terms of the nonlocality of the optical potential, but the details remain a topic of active interest [11,12] because of its impact on the interpretation of pion absorption, spectroscopy with the $(e,e'p)$ reaction, and other processes involving the propagation of nucleons in nuclei.

The purpose of the present work was to provide total cross-section data above 100 MeV for a large number of target nuclei in small bins and with good statistical and systematic accuracy. The conditions of the experiment were such that precision data were obtained simultaneously for all energies above a fixed threshold (~ 5 MeV), thus providing a single, internally consistent, precision data set that spans the traditional domains of low- and intermediate-energy nuclear physics.

II. METHOD

The high-current Target 4 facility at the Weapons Neutron Research (WNR) complex at Los Alamos National Laboratory has been described previously [13] and is treated only briefly here. Figure 1 shows the general arrangement. Part of the 800 MeV proton beam from the Los Alamos Meson Physics Facility (LAMPF) linear accelerator produces a "white" source of neutrons by spallation on a thick, water-cooled tungsten target inside a

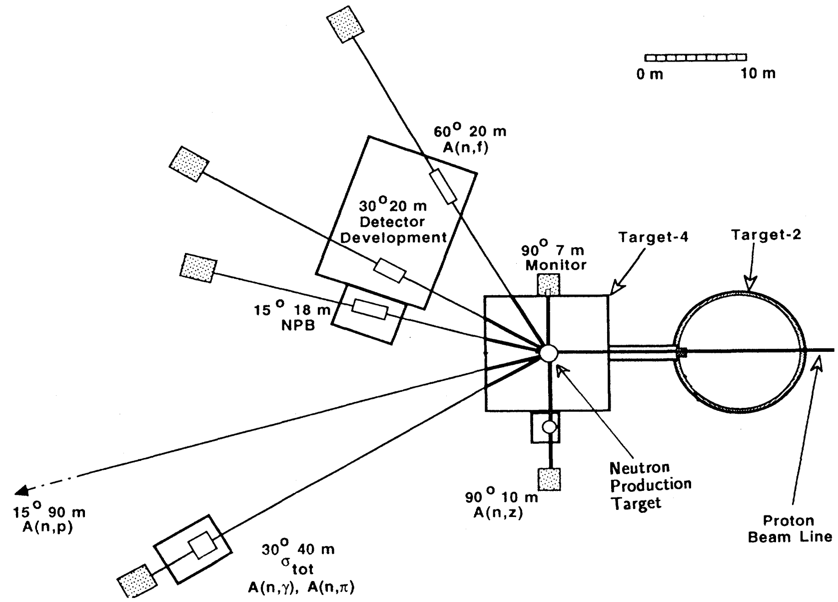

FIG. 1. Overview of the WNR fast, "white" neutron facility at Los Alamos National Laboratory. The present experiment was performed on the 30° beam line at the bottom of the figure.

massive shield of concrete and iron. Neutrons emerge along seven collimated beam lines, thus allowing simultaneous operation of several experiments. The present work was carried out on the beam line 30° to the left of the incident proton beam. At this angle the spallation spectrum extends up to 600 MeV. Total cross sections were measured in a classic "good geometry" transmission experiment. Time of flight and, consequently neutron energy, was measured as the time difference between the neutron detector *start* pulse and the delayed beam pick-off *stop* pulse.

A. Collimation, sample changer, and detector arrangement

Figure 2 shows the experimental arrangement of collimators, sweeping magnets, sample changer, monitor, and neutron detector. Collimators C1, C2, C3 (all 6.35 cm in diameter), and C6 (8.9 cm in diameter) were installed permanently. The shutter collimator C4 (1.90 cm in diameter) was almost 2 m long and defined the beam size at the sample. The 13 and 34 m collimators C5 (1.9 cm in diameter) and C7 (6.35 cm in diameter), respectively, were sleeved together with 91-cm-long commercial steel pipes. The solid angle subtended by the detector was calculated to be 9.07×10^{-7} sr.

A ^{238}U disk on the outside of the shutter was used to attenuate the γ flash by a factor of 3 while reducing the total neutron flux by 4%. Sweeping magnets (SM's) before and after the sample changer deflected charged particles from the source and sample out of the neutron flight path. Charged particles produced along the flight path were eliminated by a veto counter V. For better light collection, a tent construction [14] was chosen for the veto counter. A 10 cm$\times$10 cm, 0.16-cm-thick sheet of BC 404 was supported inside a reflective tent with sidewalls consisting of 0.16-cm-thick polished aluminum and front walls consisting of one layer of aluminum foil. The base of the tent was fixed to a Plexiglas light pipe, which, in turn, was attached to the face of a 5-cm-diam RCA 8575 photomultiplier tube (PMT) (-1800 V). The monitor M consisted of a 3.18 cm$\times$16.5 cm, 0.64-cm-thick piece of BC 404 attached directly to a photomultiplier tube (-2000 V).

A Geneva Drive rotary target changer S was used to change positions in a few seconds. It drove a 63.5-cm-diam aluminum wheel to which eight 12-cm-long or four 20-cm-long samples could be mounted. Sample holders were pinned very precisely into position. The alignment problem was reduced to getting the wheel into position once. New samples were installed in a few minutes without realignment.

Monte Carlo calculations predicted a beam spot size of 7.4 cm$\times$7.4 cm at 37 m, and a beam scan at 38.5 m showed a beam profile of 7.54 cm$\times$7.67 cm at full width at $\frac{1}{10}$ the maximum. Therefore the neutron detector was chosen to be a 8.9 cm$\times$8.9 cm, 1.27-cm-thick piece of BC 404. The scintillator was epoxied to two 11.4-cm-long Plexiglas light guides, tapering to two 5-cm-diam R329 Hamamatsu PMT's connected to EMI tube bases (-1650 and -1325 V, respectively). The tube bases were transistor stabilized to prevent gain changes during large changes in count rate.

B. Electronics

A simplified block diagram of the electronic equipment is shown in Fig. 3. The entire system was controlled by a logic T_0 signal, provided by the proton beam pick-off, one pulse for every micropulse. Micropulse spacing was constant at 1.8 μs throughout the duration of the typically 625-μs-long macropulse. The macropulse repetition rate varied from 10 to 40 Hz.

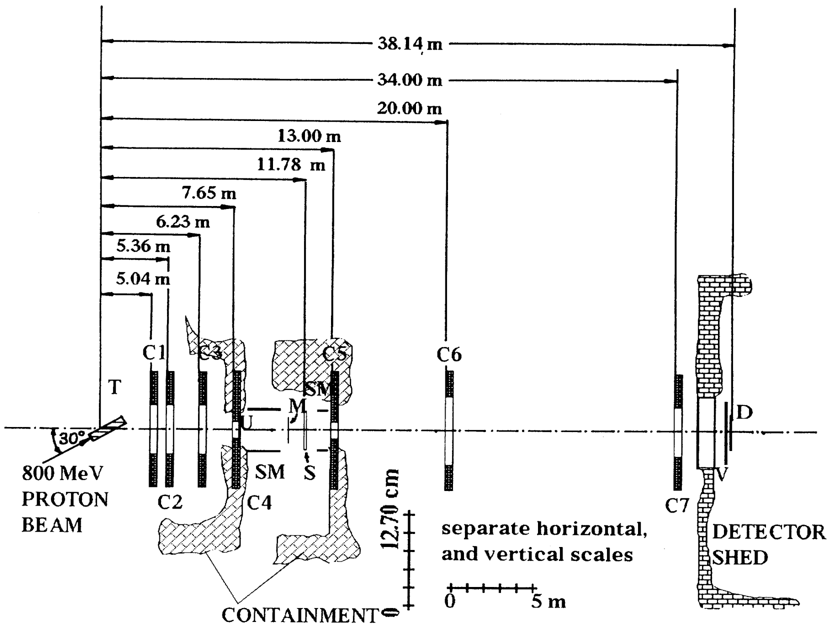

FIG. 2. Geometry for the present experiment. Note the very different horizontal and vertical scales. Collimators are denoted by C1,. . . ,C7. Sweeping magnets (SM's) deflect charged particles from the beam. Neutron flux was monitored by detector M. The sample was located at S. Transmitted neutrons were detected at D preceded by a charged-particle veto counter V.

With T_0's absent, the system remained in a dormant state. With T_0's present (scaler 0 provided the number of T_0 pulses), a 20 s timing circuit was engaged; samples were cycled at a rate of one per 20 s. Neutron detector signals were channeled into a mean timer and signal sum to provide an alternative high bias. The mean timer signal was used to start the time-to-digital converter (TDC) (LeCroy 4204). Scaler 2 provides the number of detector hits. No start signal was given if the TDC was not ready to accept data or the time interval fell outside a 1.8 μs

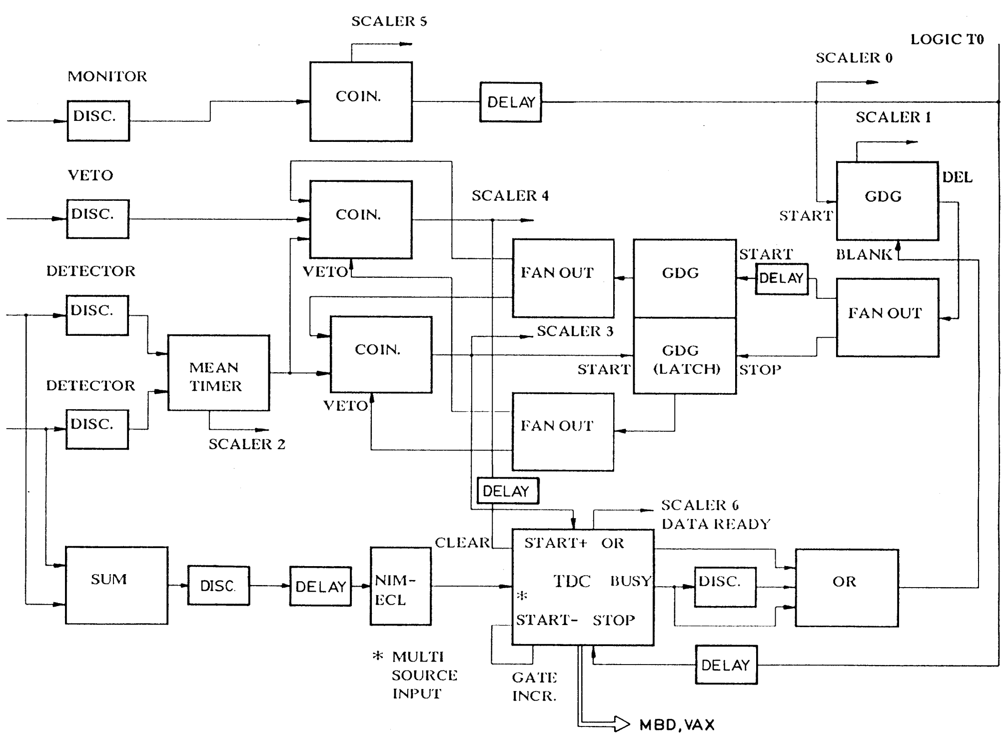

FIG. 3. Electronics block diagram. GDG denotes gate and delay generator. TDC is time-to-digital converter.

time window. Scaler 1 counted the number of live T_0's. Scaler 3 provided the number of start signals or so-called "looking time." Scaler 4 registered the number of veto counts.

In the same time frame, the summed and discriminated right-left detector signal determined under which of two different biases the event was read into the histogramming memory (LeCroy 3588). The histogramming memory consisted of 16 kilobytes of memory, 8192 channels for each bias with a channel width of 0.3125 ns. Scaler 6 provided the total number of high-differential-bias events. The monitoring system consisted of a monitor detector in coincidence with the logic T_0. Scaler 5 provided the total number of monitor counts.

After 20 s, the system was inhibited, and the content of the histogramming memory and scalers is read into preassigned data areas according to position. The sample wheel was started forward one position, the position verified, and the system inhibit lifted. If the position was not verified, data taking was halted. After every 40 positions, or 5 complete sample wheel turns constituting 1 run, the contents of the data areas were transferred onto disk file. Accumulated spectra and scaler arrays were not cleared; only data accumulated over a single run period were erased.

C. Samples

Sample diameters varied from 2.2 to 2.9 cm, according to the availability of material, to shadow completely the detector from the source. To reduce inscattering the sample was placed at a distance of $\frac{1}{3}$ the flight path. When sample properties allowed it, densities were determined in water. The physical properties of the samples are given in Table I.

Several samples ($^{90}ZrO_2$, ^{40}Ca, NaI, NaF, and CsF) had to be encapsulated in thin metal cans because of their great cost or their chemical properties in air. Matching empty cans were then used for the sample-out measurement. Typically, the difference between the open beam spectrum and the empty can spectra was less than 1%.

Whenever possible, sample lengths were chosen to optimize total counting times [15] in the energy range 100–600 MeV, for a counting statistical error of below 1%. Calculations show optimum counting times in the transmission range $0.1 < T < 0.4$, independent of background. For instance, considering Al, Al_2O_3, and AlN, 20 cm thick in the energy range 5–540 MeV ($0.04 < T < 0.7$), a 1% statistical error would have demanded a total counting time of ~ 82 d if the background were zero. On the other hand, accepting a 2% error beyond $T > 0.5$ or $T < 0.1$ would have reduced the total counting time to 3.8 d. The desired accuracy below 100 MeV (1%) in a reasonable amount of time could be reestablished by cutting the sample in half.

Special mention must be made of the Pb samples. A 326 g sample of highly enriched ^{208}Pb was available, but there was considerable reluctance to irradiating and activating the very valuable material. An alternative approach was suggested by Harvey (Oak Ridge) [16], who was in possession of two large samples of radiogenic Pb ores of very different isotopic composition (labeled R206 and R208 in Table II). By adding 29.49 g of ordinary Pb to 692.6 g of R208, the same atomic density of the isotopes 207 and 206 could be produced as already existed in the 208.5 g sample of R206. Thus the R206 sample was the proper "sample-out" compensator to obtain a true measure of σ_T (^{208}Pb) from the R208 sample. The compensator method worked to better than three significant figures in the sense that it yielded the same cross sections as the isotopically enriched sample, but with much better precision because of the greater sample mass and longer exposure times. The technique has also been described by Horen *et al.* [16]. For the other chemical compounds, no detailed effort was made to match atomic contents; e.g., the transmission of BeO was taken as a product of the transmission of Be and O.

TABLE I. Sample characteristics.

Sample	l (cm)	M or A (g/mol)	nl (at/b)
Be	20.188	9.012	2.4852
Be	10.060	9.012	1.2317
Be	2.856	9.012	0.3201
C	9.261	12.011	1.0448
Al	20.527	26.982	1.2349
Si	20.385	28.086	1.0177
^{40}Ca	5.746	39.963	0.1299
Cu	6.000	63.546	0.5067
Cu	11.905	63.546	1.0053
Nb	10.422	92.906	0.5793
Sn	8.927	118.690	0.3297
Ta	8.148	180.948	0.4518
Bi	11.193	208.980	0.3153
^{208}Pb	5.648	207.977	0.1861
BeO	7.336	25.012	0.4881
AlN	20.348	40.988	0.8369
AlN	7.894	40.988	0.3246
CaF_2	20.340	78.077	0.4961
Al_2O_3	20.360	101.961	0.4645
Al_2O_3	7.880	101.961	0.1813
$^{90}ZrO_2$	19.063	121.904	0.1766
R206	3.655	206.166	206: 0.105 92
			207: 0.010 26
			208: 0.003 57
R208	208: 12.071	207.467	206: 0.106 12
plus			207: 0.010 24
natural Pb	N 0.514	207.241	208: 0.295 52
CsI	10.165	259.810	
NaF	10.160	41.988	
NaI	10.160	149.894	
CsF	10.160	151.904	

TABLE II. Isotopic composition of the Pb samples.

Name	Isotopic abundance (%) 204	206	207	208
^{208}Pb				99.17–99.75
R206	<0.05	88.46	8.57	2.98
R208	<0.5	25.82	1.65	72.53
Natural Pb	1.4	24.1	22.1	52.4

III. PERFORMANCE

A. Open beam spectrum

Figure 4 shows a typical open beam spectrum with data for low and high differential biases added. The biases were 2.96 MeV for the low bias to eliminate the low-energy background and 9 MeV for the high bias. The spectrum was accumulated over 1.78×10^4 s. The energy range of measurement was from 2.96 MeV, which is just 0.9 MeV above the frame overlap threshold, to 600 MeV. However, the roll-off in detector efficiency near the threshold leads to large statistical errors below 5 MeV. The typical counting rate from 5 to 570 MeV is at least one count per second per channel. The uncertainty of the γ-peak centroid was found to be ±0.156 ns, and its full width at half maximum (FWHM), which determines the overall energy resolution of the system, is 0.75 ns.

B. Flight path determination

To determine the length of the flight path, well-known resonances in the beam spectrum transmitted through carbon and the γ-peak position are used. Figure 5 shows the C transmitted beam spectrum with the corresponding resonance energies, and a channel width of 0.3125 ns. The neutron energy is given by $E_n=m_nc^2[1/(1-\beta_n^2)^{1/2}-1]$ or solving for

$$\beta_n=[1-1/(E_n/m_nc^2+1)^2]^{1/2} .$$

But $\beta_n=v_n/c=L/c_t$, where L is the length of the flight path and t the neutron time of flight. t is the time difference between *start* and *stop* given by $t=c_\gamma\tau+L/c-c_n\tau$, where c_γ and c_n are channel numbers and τ is the channel width (0.3125 ns). The first two terms are an expression of the relative start time and the last term the expression of the relative stop time. Substituting for t and solving for $c_\gamma-c_n$ lead to

$$c_\gamma-c_n=\frac{L}{c\tau}\left[\frac{1}{[1-1/(E_n/m_nc^2+1)^2]^{1/2}}-1\right], \qquad (1)$$

which is the form $y=kx$. A least-squares fit yields a flight path of 38.14 m.

IV. DATA REDUCTION

All data reduction, save the flight path determination, was done using a FORTRAN program (WNRVAX.FOR) written for the purpose of total cross-section determination, which also includes error propagation. Open beam and sample spectra γ peaks are shifted to coincide. A typical corrected (corrections given below) open beam spectrum is shown in Fig. 4.

A. Analytic dead time correction

The analytic dead-time correction takes into account that low-energy neutrons have a smaller probability of being counted than high-energy neutrons. Taking into account variations of the beam intensity, it can be shown [17] that the analytic dead time correction for the number of counts in channel i is given by

$$N_c(i)=N_{T_0}\frac{-\ln\left\{1-[N_0(i)/N_{T_0}]\Big/\left[1-\sum_{j=i+1}^{M}N_0(j)/N_{T_0}\right]\right\}}{1-\sigma\tanh\left[\sigma\sum_{j=i+1}^{M}N_c(j)/N_{T_0}\right]} . \qquad (2)$$

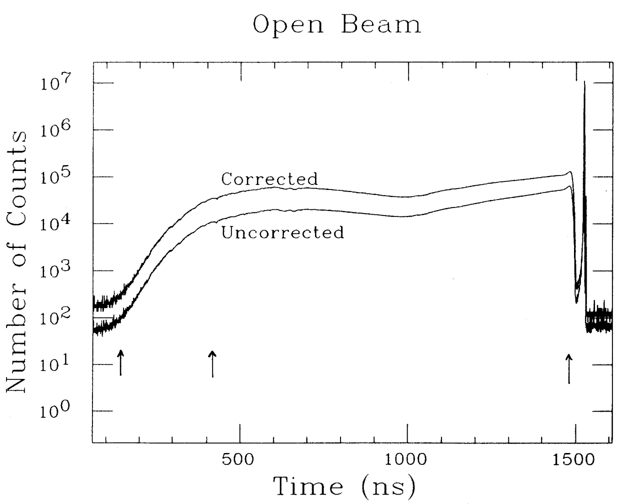

FIG. 4. Sharp peak on the right is the gamma flash. The arrows indicate (left to right) the location of neutrons of kinetic energy 2.96, 5, and 570 MeV.

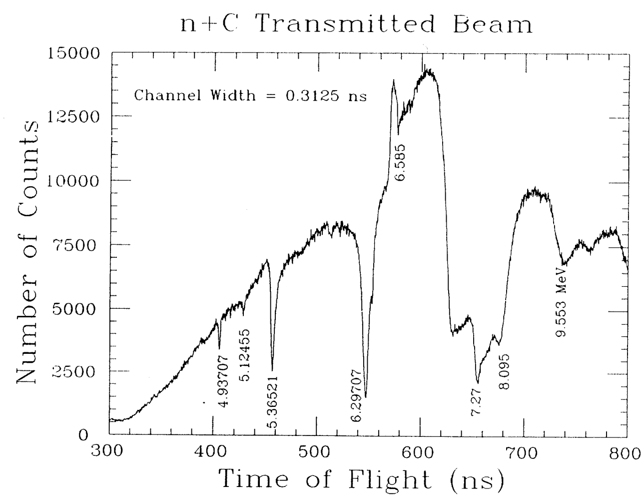

FIG. 5. Spectrum of neutrons transmitted through the graphite sample. Neutron energies (in MeV) at several points in the spectrum are given.

N_{T_0} is the number of logic T_0's, $N_0(i)$ is the number of observed counts in channel i, M the maximum channel number, and σ^2 is the relative variance of the beam intensity. The first-order analytic dead time correction [$\sigma=0$ in Eq. (2)] yields correction factors applied to the observed number of counts as high as 1.7. Inclusion of beam intensity variation in the dead time correction altered analytic dead time correction factors by less that 0.1%. σ was determined by randomly sampling a signal proportional to the beam intensity (T_0 linear) with the aid of a radioactive source.

B. 1 μs Block correction, normalization, and background

While events are being processed by the data acquisition system, no other events can be accepted. By knowing the total number of logic T_0's (scaler 0), the number of times the system was alive, and the number of live T_0's (scaler 1), the true spectra are obtained by multiplication of $N_{T_0}/N_{T_0\text{ live}}$. The factor is typically between 1.1 and 1.8. The scalar value of $N_{T_0\text{ live}}$ is corrected for the number of veto counts in scaler 4.

The spectra are normalized to the monitor counts, and the time-independent background is subtracted. Using the two-sample technique [18], the time-dependent background was extracted and found negligible. The open beam and target time-of-flight spectra are converted into energy-dependent spectra. Inscattering and beam hardening effects were also negligible in the present experiment.

C. Binning and averaging

The useful part of a typical time-of-flight spectrum contains over 3400 channels of data corresponding to neutron energies between 5 and 600 MeV, and so there is some flexibility in the choice of binning functions. Very small bins emphasize the fluctuations in level density at high excitation energy—a topic for future study. For the present report, we choose to average over some of these fluctuations in order to prepare an "optical model file" for which the bin width (ΔE) is 1% of the bin energy E.

Another choice to be made in the analysis is between the accumulated files and scalar readings and the averages of the individual 15 min runs. During the course of the experiment, it was convenient to monitor the results by calculating the cross sections from the accumulated files. Afterward, a detailed run-by-run analysis was performed for several of the targets. In these lengthy calculations, the individual transmissions were calculated and averaged using the same dead time correction procedure as for the on-line calculations with the accumulated files. No differences (at the 0.5% level) were found between the cross sections obtained in the run-by-run analysis and those from the accumulated files.

V. RESULTS

Results from the present experiment are summarized in Fig. 6, where the 474 individual measurements for each nucleus are connected with lines and the error bars are suppressed. The most prominent feature of Fig. 6 is the systematic behavior of the peaks and valleys as a function of E and A—sometimes called the nuclear Ramsauer effect. Another obvious feature is the disappearance of sharp compound nuclear resonances with increasing E and A. Also evident is the absence of any great change in the total cross section near the pion production threshold. All targets show a gentle increase in the total cross section above a minimum near 300 MeV, which is due to pion production. The slope of that increase is somewhat larger for nuclei with $N>Z$, which

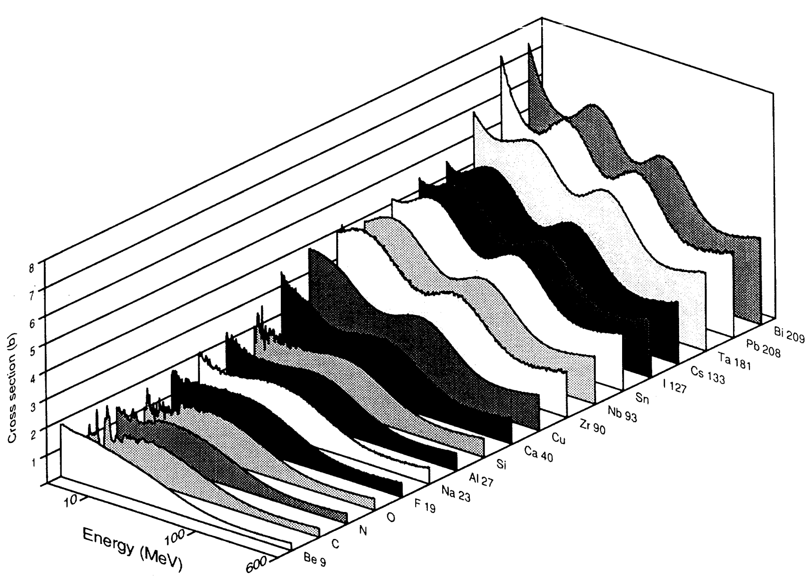

FIG. 6. Overview of results from the present experiment. For clarity, the data sets are equally spaced along a false A axis.

might be understood in terms of Δ formation in the nucleus.

A. Counting statistics

Errors due to counting statistics are summarized in Fig. 7, where $\Delta\sigma/\sigma$ is shown as a function of energy for three cases. The curve for Cu is typical of the results for metal targets. The best results were obtained from the radiogenic Pb samples, as shown by the lowest curve in Fig. 7. The worst results ($\Delta\sigma/\sigma \sim 4\%$ for $E > 200$ MeV) were obtained for ^{40}Ca. The small mass of the separated isotope sample (54 g) did not permit a better measurement in the time available. Unfortunately, this region of large statistical error propagates through into the determination of the cross section for Na, F, Cs, and I.

The neutron total cross section for oxygen was determined independently with samples of Al_2O_3 and BeO. The two data sets were in excellent agreement, and so they were merged into a single data set, which was then used to obtain the ^{90}Zr cross sections from measurement on $^{90}ZrO_2$.

B. Systematic errors and renormalizations

Measured transmissions were converted into cross sections by the familiar relationship

$$\sigma_x = -\frac{1}{nl}\ln T_x ,$$

where T_x is the transmission of the sample and nl is the number of atoms per unit area. Rapid cycling of the samples and stable fast electronics contributed to the successful measurement of the transmission (except for ^{40}Ca above 200 MeV), and so the accuracy of the cross section is given directly by the accuracy with which the areal density is known. For elemental metal targets, this quantity is readily determined to better than 0.5%. However, for a few targets, this number was difficult to determine.

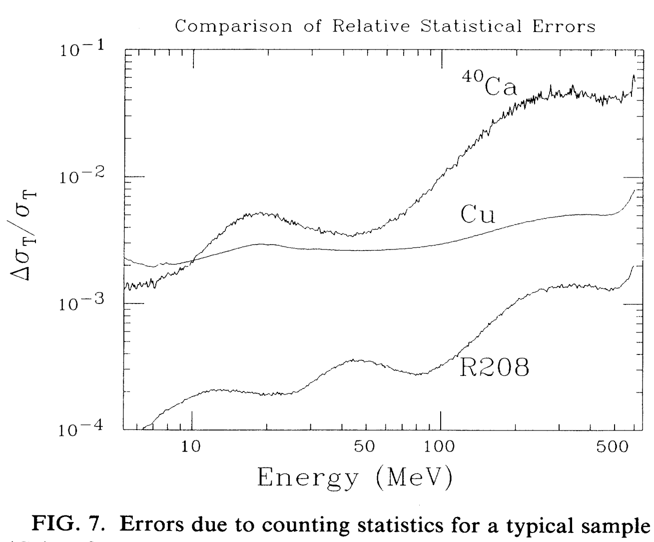

FIG. 7. Errors due to counting statistics for a typical sample (Cu), a favorable sample (R208), and an extremely thin sample (^{40}Ca).

Each case requires brief comment.

^{40}Ca.—This sample was prepared and sealed in a stainless-steel can over 20 years ago, and the mass numbers written on the container were clearly erroneous. We renormalized our transmission measurements upward by 2% to two compatible Ca measurements below 80 MeV from Oak Ridge National Laboratory [19,20].

^{90}Zr.—The ZrO_2 was an extremely fine white powder which resisted efforts to compress it into a stainless steel can. The material seems to have settled into a somewhat higher density during the course of the experiment. We renormalized our results downward by 2.5% to agree with a recent ENDF B-VI evaluation [21].

N.—Fine AlN powder was hot pressed into a cylinder in a N_2 atmosphere. The manufacturer states that it contains an unknown amount of excess nitrogen interstitially. We renormalized our results downward by 5% to obtain excellent agreement with the National Bureau of Standards results [22].

The alkalai halide samples were especially difficult to characterize. For example, the manufacturer recommended a value for the density of the encapsulated CsF sample that was 12.7% higher than the standard handbook value. Since the cross-section determination for each of these nuclei was influenced by the poor counting statistics of ^{40}Ca experiment, final values for these cross sections are being withheld pending a renormalization in progress. Results are shown in Fig. 6 for illustration only and were not included in any of the calculations described in Sec. VI.

For all of these renormalized cases (^{40}Ca, ^{90}Zr, and N), we assign a normalization uncertainty of 3%.

C. Intercomparison

The present data could be compared with hundreds of earlier works, but such comparisons often become cluttered and uninformative. Moreover, comparison of two data sets in the resonance region is meaningful only if the resolutions are comparable. The present work was intentionally averaged into rather wide bins at low energy in order to suppress some of the fluctuations. In Fig. 8 we compare our results with earlier work on ^{12}C at the WNR facility from 5 to 220 MeV [23] and with the work of Franz *et al.* [3] from 160 to 575 MeV. The present work is seen to be in excellent agreement with the others. In Fig. 9 we compare the present results for Cu with the work of Larson [20] between 5 and 80 MeV and with Ref. [3] above 160 MeV. Again, agreement is good, thus confirming the accuracy of the data of Ref. [3] that were obtained with a totally different and rather difficult technique.

The present data should be useful in a variety of applications, e.g., optical model studies, radiation dosimetry, transport, and shielding. The precision and detail of the data represent a major improvement in the present state of the art. The numerical data files (with $\Delta E/E = 0.01$) have been deposited in the National Nuclear Data Center at Brookhaven National Laboratory. Specialists who are interested in higher-resolution data in the resonance region should contact the authors.

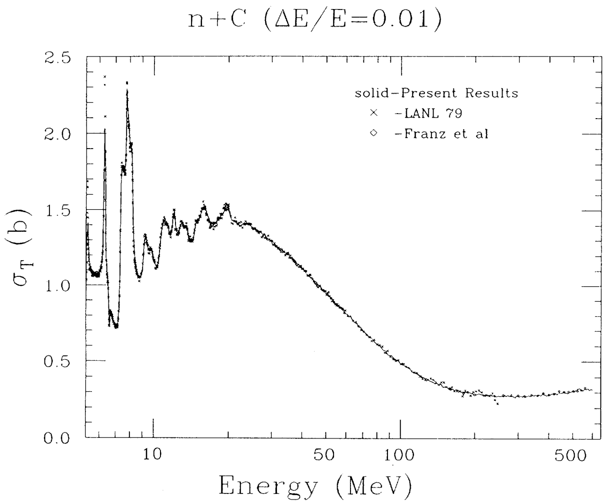

FIG. 8. Present results for carbon (solid line) compared with earlier work from Refs. [3] and [23]. The seemingly better resolution of the 1979 data is a consequence of the choice of binning function for the present work. The resolution of the unbinned raw data is about a factor of 2 better than the 1979 work.

VI. DISCUSSION

A. Parametrizations of the cross sections

In this section we present some elementary parametrizations of the cross sections above 100 MeV. The presentation follows closely the analysis by Franz *et al.* [3] and extends that work primarily by including many more cross-section measurements most (except for ^{40}Ca) with error bars smaller by a factor of 2 or so. The data set includes 14 elements between Be ($A=9$) and Bi ($A=209$). The alkalai halides were not included in the analysis.

First, we consider a simple factorization into an "elementary" cross section and an A-dependent term:

$$\sigma(A,E_n)=\sigma_0(E_n)A^{\beta(E_n)}, \tag{3}$$

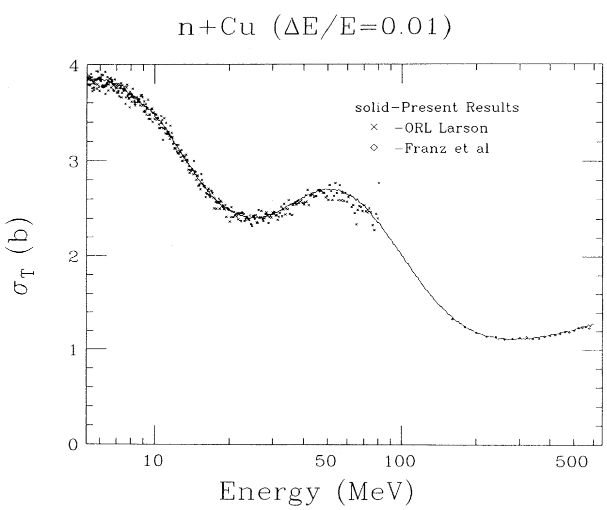

FIG. 9. Present results for copper (solid line) compared with earlier work from Refs. [3] and [20].

where σ_0 is an averaged nucleon-nucleon cross section at kinetic energy E_n and $\beta(E_n)$ is a measure of the shadowing of the nucleus. Figure 10 shows a typical fit to the cross-section data at 320 MeV, and Fig. 11 shows the energy dependence of the two parameters. The results in Fig. 11 are in excellent agreement with those in Fig. 6 of Ref. [3], thus supporting the same general conclusions: (i) The nuclear transparency lies between the extreme values of a black nucleus ($\beta=\frac{2}{3}$) and a nucleus without shadowing ($\beta=1$). Moreover, the nuclear transparency decreases with increasing energy in this energy region. (ii) The minimum in $\sigma_0(E_n)$ occurs at significantly lower energy than the minimum in the isospin-averaged free nucleon-nucleus cross section. This shift incorporates the effects of the Fermi momentum of the struck nucleon, Pauli blocking, and other "medium modifications" of the nucleon-nucleus interaction and might be a useful benchmark for theories that seek to go beyond the impulse approximation. In contrast with Ref. [3], the present data show a definite departure of the measured cross sections from Eq. (3) for nuclei with $A<20$, at all energies. Significantly better fits (leading to the parameters shown in Fig. 11) were obtained for $A\geq 27$.

An alternative two-parameter description of the total cross-section data can be given in terms of a nuclear size parameter R and an absorption coefficient K. For a partially transparent disk, one expects

$$\sigma=2\pi R^2(1-e^{-KR}), \tag{4}$$

where $R=r_0A^{1/3}$. The generalization to a spherical target is given by [24]

$$\sigma=2\pi R^2\{1-2[1-(1+KR)\exp(-KR)]/K^2R^2\}. \tag{5}$$

Interpretation of the reciprocal of K in terms of the mean free path requires some care in view of the extensive discussions of this quantity for the proton-nucleus in-

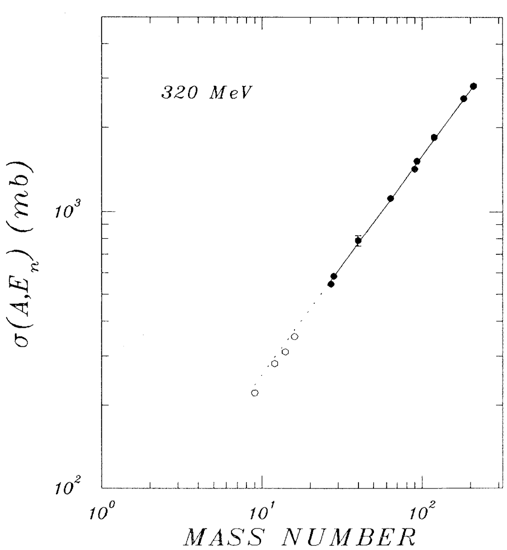

FIG. 10. Fit to the total neutron cross sections at 320 MeV with Eq. (3). Only nuclei with $A\geq 27$ (solid circles) were used to determine the parameters.

teraction and the specific meaning of the mean free path in reaction theory. References [8–12] provide an introduction to the recent literature. Negele [25] describes the need to find a bridge between the formal quantity used by theorists and the experimentalists' operational definition of exponential attenuation of flux. Many authors (e.g. [25,26]) point out the great sensitivity of the mean free path ($\Lambda=1/K$) to any assumptions made about R. In this section we investigate the sensitivity of Λ to two different applications of Eq. (5). No assumptions are made about the energy dependence of R ($=r_0 A^{1/3}$). R is determined simultaneously with Λ by least-squares fitting to 14 measurements of the total cross section at each of 180 values of the neutron kinetic energy. The two forms of Eq. (5) are (a) Eq. (5) as given with $R=r_0 A^{1/3}$ and (b) replacement of R in Eq. (5) with $R'=r'_0 A^{1/3}+\lambda\!\!\!^{-}$, where $\lambda\!\!\!^{-}$ is the reduced de Broglie wavelength of the projectile.

In either case, fits to Eq. (5) are considerably better for light nuclei than were fits to Eq. (3), at least for the higher energies in this study. A typical case is shown in Fig. 12. Below about 160 MeV, the fit deteriorates rapidly, and Eq. (5) is considered to be unreliable for the extraction of mean free path. One reason for this failure is that the form of Eq. (5) is only justified for a purely absorptive nucleus [24,27], i.e., for the real part of the optical potential equal to zero. This approximation might be reasonable for $400 \lesssim E_n \lesssim 600$ MeV, but is clearly false for $E_n < 160$ MeV. At this time, however, we lack sufficient information about the neutron-nucleus optical potential to make the numerical corrections to Eq. (5). Moreover, Meyer and Schwandt [28] have shown how different optical model parametrizations can lead to greatly differing values for the mean free path because of the acute sensitivity of Λ to assumptions about R. Thus we take a purely empirical approach: Wherever Eq. (5) fits the data for all nuclei, we use it to extract R and Λ.

Results are shown in Figs. 13 and 14, where Λ and r_0 are shown as functions of E_n both including (solid circles) and omitting (open circles) the reduced de Broglie wavelength. The open squares show the same information for the proton-nucleus interaction from an analysis of proton reaction cross sections [29] in which the reduced de Broglie wavelength was included in a formula analogous to Eq. (5). It is clear that the mean free path is sensitive to the inclusion of the reduced de Broglie wavelength. The open circles are in good agreement with Ref. [3], which omitted $\lambda\!\!\!^{-}$, while the solid circles are in good agreement with proton-nucleus mean free paths. An extended discussion of empirical nucleon-nucleus mean free paths and the optical model is planned to be published separately [30].

B. Neutron-nucleus optical model

One major goal of the present work was to contribute to the development of the neutron-nucleus optical poten-

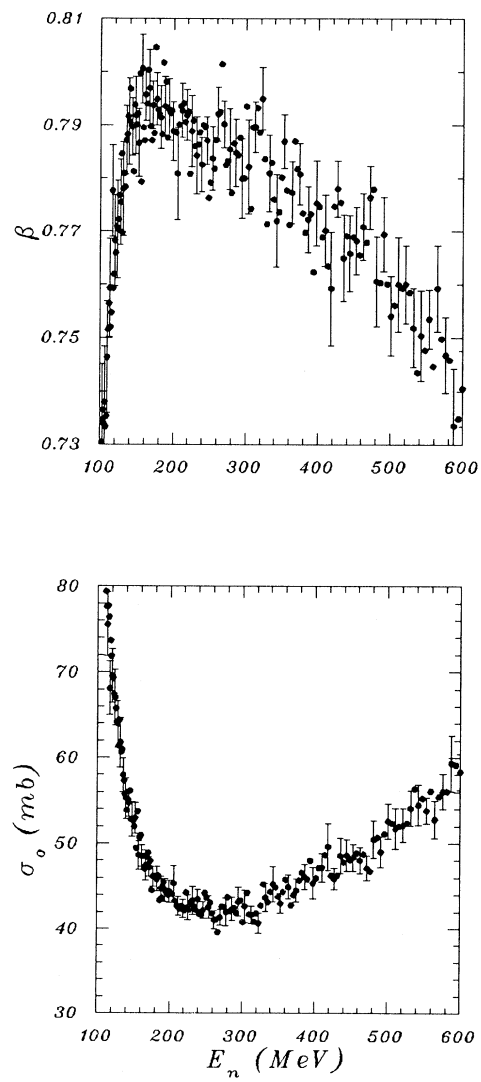

FIG. 11. Energy dependence of the parameters β and σ_0 of Eq. (3).

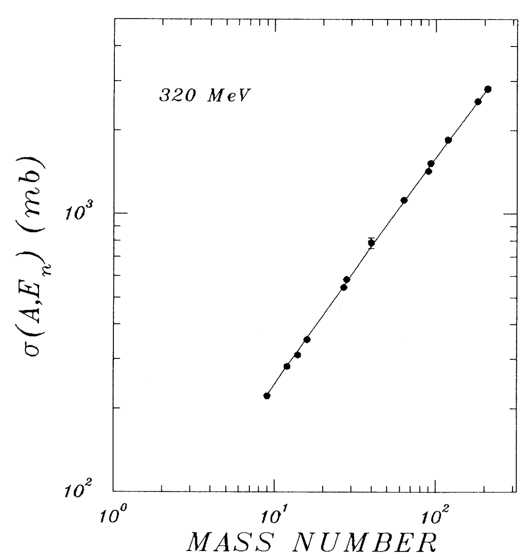

FIG. 12. Fit to the total neutron cross sections at 320 MeV for fourteen samples. Equation (5) with $\lambda\!\!\!^{-}$ included was used. The points for ^{208}Pb and ^{209}Bi are indistinguishable in the figure.

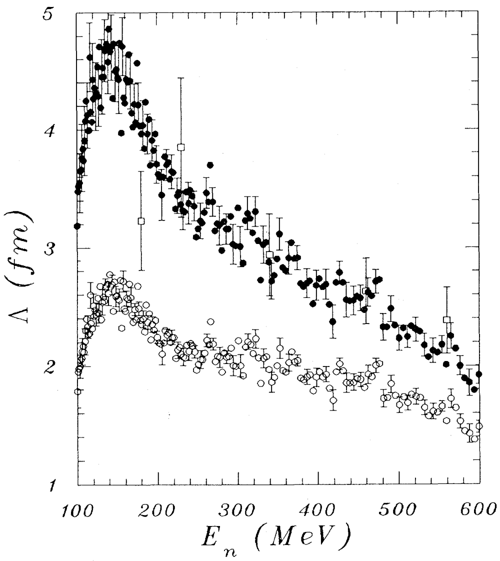

FIG. 13. Energy dependence of the fitting parameter Λ of Eq. (5). Solid circles were obtained with the reduced de Broglie wavelength ($\lambda\!\!\!^{-}$) included. Open circles were obtained with $\lambda\!\!\!^{-}$ omitted. The open squares were obtained from analysis of proton reaction cross sections [29] which included $\lambda\!\!\!^{-}$. Below 160 MeV, the association of Λ with mean free path is unreliable.

tial. This work is still in progress, but a few preliminary observations are in order. First, the highly successful Ohio State description of proton-nucleus scattering based on Dirac phenomenology [7] is one of the very few models that attempt to cover the entire range of the present data. It can be used to calculate neutron scattering by setting the Coulomb potential to zero. This approach is able to predict the energy dependence of the neutron total cross section from 20 to 600 MeV with no further adjustment of the parameters [31]—but only for $N=Z$ nuclei. Nuclei with neutron excess (^{90}Zr and ^{208}Pb) are not so well described. This suggests that the isoscalar interaction is correctly given in this model, but that the isovector interaction is not. The specific dependence of the parameters on radius and mass number is not appropriate for neutron scattering from heavy nuclei.

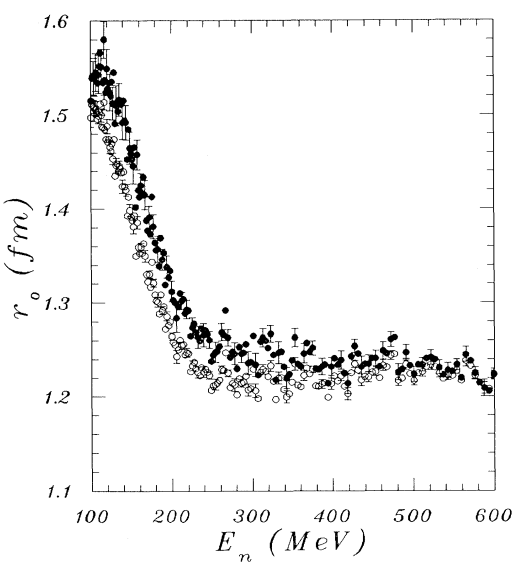

FIG. 14. Energy dependence of the fit parameters r_0 of Eq. (5) including (solid circles) and omitting (open circles) the reduced de Broglie wavelength.

At lower energy the nonrelativistic optical potential of Jeukenne, Lejeune, and Mahaux [32] provides a nearly parameter-free description of the present data within its limits of validity (i.e., $E_n \lesssim 140$ MeV)—but again only for $N \approx Z$ nuclei. Predictions for ^{208}Pb [33] are distinctly less successful, which further points to problems with the isovector part of the nucleon-nucleus interaction.

Finally, calculations with the relativistic impulse approximation [6], which invoke charge symmetry of the nucleon-nucleus interaction in order to calculate neutron scattering observables, provide a good description of the total cross sections for $E_n > 200$ MeV without further adjustment of the parameters [34], but the isovector part of the interaction is not well determined.

VII. CONCLUSION

The LAMPF WNR facility provides an extremely powerful tool for measurements of the kind described here. Very high neutron flux over a wide range of neutron energies not only facilitates accurate measurements in the intermediate-energy regime, it also establishes a new standard of precision at lower energy. Thirteen samples were measured to very high precision, one sample (^{40}Ca) to modest precision, while five other samples (F, Na, Ca, I, and Cs) require renormalization.

A simple factorization of the cross-section data into an energy-dependent elementary cross section and an A-dependent term was shown to fail for the light nuclei. For heavy nuclei, interesting information on medium modification and shadowing [3] has been extended and refined. A partially-transparent-sphere model of the nucleus permits extraction of the nucleon-nucleus mean free path in much greater detail than has been available prior to this experiment. The extraction, however, is model dependent. Proton and neutron mean free paths are in good agreement above 200 MeV provided that the same model is used to derive the empirical values from the data. Much of the early concern about the nucleon mean free path [8–10] may have been due to a meager database for proton reaction cross sections [26,29] and the aforementioned model dependence [25,26,28]. A firm empirical basis for the nucleon-nucleus mean free path above 160 MeV is an important result of the present work.

Finally, preliminary analysis of the present data in terms of various optical models indicates that the nucleon-nucleus interaction is not yet a solved problem and that major issues concerning the isovector character of the interaction remain unresolved.

ACKNOWLEDGMENTS

The generous assistance of D. J. Horen, J. A. Harvey, and the technical services group at Oak Ridge National Laboratory in providing several of the targets is gratefully acknowledged. Preliminary calculations of neutron cross sections with the phenomenological Dirac proton potential by S. Hama are especially appreciated, as are the many fruitful discussions with B. C. Clark, K. H. Hicks, and S. M. Grimes. The work was supported in part by the National Science Foundation via Grant No. PHY-88-10220 and in part by the Department of Energy under Contract No. W-7405-ENG-36.

[1] V. McLane, C. L. Dunford, and P. F. Rose, *Neutron Cross Sections* (Academic, San Diego, 1988), Vol. 2.

[2] W. Schimmerling, T. J. Devlin, W. W. Johnson, K. Vosburgh, and R. Mischke, Phys. Rev. C 7, 248 (1973).

[3] J. Franz, H. P. Gross, L. Lehmann, E. Rössle, H. Schmitt, and L. Schmitt, Nucl. Phys. **A490**, 667 (1988).

[4] H. F. Arellano, F. A. Brieva, and W. G. Love, Phys. Rev. C **41**, 2188 (1990).

[5] Ch. Elster, T. Cheon, E. F. Redish, and P. C. Tandy, Phys. Rev. C **41**, 814 (1990).

[6] C. J. Horowitz, D. P. Murdock, and B. D. Serot, in *Computations in Nuclear Physics,* edited by K. Langanke, J. A. Maruhn, and S. E. Koonin (Springer-Verlag, Berlin, 1991), p. 129.

[7] S. Hama, B. C. Clark, E. D. Cooper, H. S. Sherif, and R. L. Mercer, Phys. Rev. C **41**, 2737 (1990); R. Kozak and D. G. Madland, *ibid.* **39**, 1461 (1989); Nucl. Phys. **A509**, 664 (1990).

[8] J. P. Schiffer, Nucl. Phys. **A335**, 339 (1980).

[9] J. W. Negele and K. Yazaki, Phys. Rev. Lett. **47**, 71 (1981).

[10] S. Fantoni, B. L. Friman, and V. R. Pandharipande, Phys. Lett. **104B**, 89 (1981).

[11] T. Cheon, Phys. Rev. C **38**, 1516 (1988).

[12] V. R. Pandharipande and S. C. Pieper, Phys. Rev. C **45**, 791 (1992).

[13] P. W. Lisowski, C. D. Bowman, G. J. Russell, and S. A. Wender, Nucl. Sci. Eng. **106**, 208 (1990).

[14] M. L. Evans, G. Glass, J. C. Hiebert, Mahavir Jain, R. A. Kenefick, L. C. Northcliffe, B. E. Bonner, J. E. Simmons, C. W. Bjork, P. J. Riley, H. C. Bryant, C. G. Cassapakis, B. Dieterle, C. P. Leavitt, D. M. Wolfe, and D. W. Werren, Phys. Rev. C **26**, 2525 (1982).

[15] E. J. Burge, Nucl. Instrum. Methods **144**, 547 (1977).

[16] D. J. Horen, C. H. Johnson, J. L. Fowler, A. D. MacKellar, and B. Castel, Phys. Rev. C **34**, 429 (1986); J. A. Harvey (private communication).

[17] M. S. Moore, Nucl. Instrum. Methods **169**, 245 (1980).

[18] O. D. Simpson, R. G. Fluharty, M. S. Moore, N. H. Marshall, F. B. Simpson, G. E. Stokes, T. Wantanabe, and T. E. Young, Nucl. Instrum. Methods **30**, 293 (1964).

[19] F. G. Perey, Oak Ridge National Laboratory Report No. ORNL 4823, 1972.

[20] D. C. Larson, in Proceedings of the Symposium of Neutron Cross Sections from 10 to 50 MeV, edited by M. R. Bhat and S. Pearlstein, Report No. BNL-NCS-51245, 1980, p. 277.

[21] A. B. Smith (private communication).

[22] R. B. Schwartz, R. A Schrack, and H. T. Heaton II, Natl. Bur. Stand. Misc. Publ. No. 138 (U.S. GPO, Washington, D.C., 1974).

[23] P. W. Lisowski, M. S. Moore, G. L. Morgan, and R. E. Shamu, in *Proceedings of the International Conference on Nuclear Cross Sections for Technology,* Natl. Bur. Stand. (U.S.) Spec. Publ. No. 594, edited by J. L. Fowler, C. H. Johnson, and C. D. Bowman (U.S. GPO, Washington, D.C., 1980), p. 524.

[24] V. A. Nedzel, Phys. Rev. **94**, 174 (1954).

[25] J. W. Negele, Comments Nucl. Part Phys. **12**, 1 (1983).

[26] A. Nadasen, P. Schwandt, P. P. Singh, W. W. Jacobs, A. D. Bacher, P. T. Debevec, M. D. Kaitchuck, and J. T. Meek, Phys. Rev. C **23**, 1023 (1981).

[27] S. Fernbach, R. Serber, and T. B. Taylor, Phys. Rev. **75**, 1352 (1949).

[28] H. O. Meyer and P. Schwandt, Phys. Lett. **107B**, 353 (1981).

[29] P. U. Renberg, D. F. Measday, M. Pepin, P. Schwaller, B. Favier, and C. Richard-Serre, Nucl. Phys. **183**, 81 (1972).

[30] B. C. Clark, E. D. Cooper, S. Hama, R. W. Finlay, and T. Adami, Phys. Lett. (submitted).

[31] R. W. Finaly, G. Fink, W. Abfalterer, P. W. Lisowski, G. L. Morgan, and R. C. Haight, in *Proceedings of the International Conference on Nuclear Data for Science and Technology,* edited by S. M. Qaim (Springer-Verlag, Berlin, 1992), p. 720.

[32] J. P. Jeukenne, A. Lejeune, and C. Mahaux, Phys. Rev. C **16**, 80 (1977).

[33] A. E. Feldman, R. W. Finlay, W. Abfalterer, and F. S. Dietrich, Bull. Am. Phys. Soc. **37**, 1294 (1992).

[34] R. W. Finlay and Yanhe Jin, Bull. Am. Phys. Soc. **37**, 1294 (1992).